International Journal of Nanomedicine

Dovepress
Taylor & Francis Group

Open Access Full Text Article

ORIGINAL RESEARCH

Delivery of miR-26a-5p by Subcutaneous Adipose Tissue-Derived Extracellular Vesicles Alleviates Acute Lung Injury in Mice Through CHUK/NF-κB Pathway

Yu Xie[1,2,*], Liuyi Ran[2,*], Ciquan Yue[1,2,*], Chenxing Wang[1,2], Fengming Chen[3], Yadong Su[1,2], Yin Qin[1,2], Qiuhong Zhang[1,2], Jie Liu[1,2], Ning Du[2], Li Zhang[4], Yu Jiang[5], Gang Liu[1,2]

[1]Department of Emergency and Critical Care Medicine, University-Town Hospital of Chongqing Medical University, Chongqing, 401331, People's Republic of China; [2]Medical Sciences Research Center, University-Town Hospital of Chongqing Medical University, Chongqing, 401331, People's Republic of China; [3]Hubei University of Traditional Chinese Medicine Affiliated Shiyan Hospital, Shiyan, 442000, People's Republic of China; [4]Basic Research Laboratory of Traditional Chinese Medicine, Chongqing Hospital of Traditional Chinese Medicine, Chongqing, 400011, People's Republic of China; [5]Department of Respiratory and Critical Care Medicine, University-Town Hospital of Chongqing Medical University, Chongqing, 401331, People's Republic of China

*These authors contributed equally to this work

Correspondence: Yu Jiang; Gang Liu, Email jiangyu@cqmu.edu.cn; lg@cqmu.edu.cn

Background: Acute respiratory distress syndrome (ARDS) is characterized by diffuse lung injury and high mortality rates due to severe inflammation. Adipose tissue, functioning as both an endocrine and immune organ, plays a crucial role in immune regulation by secreting a variety of adipokines. Among these, adipose tissue-derived extracellular vesicles (EVs) have emerged as novel mediators of intercellular communication, capable of delivering bioactive molecules such as microRNAs to target cells. This study aimed to elucidate the immunomodulatory roles and underlying mechanisms of adipose tissue-derived EVs in the pathogenesis of ARDS.

Methods: Subcutaneous adipose tissue extracellular vesicles (SAT-EVs) were collected from the mice via ultracentrifugation. C57BL/6 mice were administered SAT-EVs (1×10^9 particles per mouse) via tail vein injection, followed by an intraperitoneal Lipopolysaccharide (LPS) injection three hours later to induce acute respiratory distress syndrome (ARDS). The mice were euthanized after 18 h to evaluate the permeability of the microvessels and level of inflammation in the lungs. For in vitro experiments, RAW 264.7 macrophages were stimulated with LPS, with or without SAT-EVs, as a control, to evaluate the inflammatory response of the macrophages.

Results: SAT-EVs treatment enhanced the survival rate of ARDS mice and reduced pulmonary vascular permeability. SAT-EVs were internalized by alveolar macrophages, leading to an attenuation of inflammation, as indicated by decreased levels of TNF-α, IL-1β, iNOS, PTGS2, and CCL2. Notably, SAT-EVs transferred miR-26a-5p to alveolar macrophages, which directly targeted conserved helix-loop-helix ubiquitous kinase (CHUK), a key regulator of the NF-κB pathway. This inhibition resulted in reduced transcription of inflammatory mediators (iNOS, PTGS2, and IL-1β). In vitro, SAT-EVs were internalized by RAW 264.7 macrophages, leading to the suppression of LPS-induced inflammation, as shown by decreased expression of TNF-α, IL-1β, iNOS, PTGS2, and CCL2. These findings suggest that miR-26a-5p plays a crucial role in the anti-inflammatory effects of SAT-EVs by suppressing CHUK and modulating the NF-κB pathway.

Conclusion: SAT-EVs significantly attenuated LPS-induced ARDS, potentially through the CHUK/NF-κB pathway mediated by miR-26a-5p, thereby exerting protective effects against inflammatory lung injury. These findings provide mechanistic insights into the role of SAT-EVs in immune modulation and suggest their potential as a therapeutic strategy for ARDS.

Keywords: adipose tissue-derived extracellular vesicles, inflammation, CHUK, acute respiratory distress syndrome, miR-26a-5p

Received: 17 January 2025
Accepted: 29 April 2025
Published: 10 May 2025

Introduction

Acute respiratory distress syndrome (ARDS) is characterized by severe, diffuse pulmonary inflammation associated with immune imbalance.[1] The primary etiological factors include bacterial pneumonia, severe trauma, and sepsis,[2–4] all of which can induce a cytokine storm, compromise the alveolar-capillary barrier, and result in extensive lung injury.[5] Lipopolysaccharide (LPS), the predominant endotoxin of Gram-negative bacteria, is a critical mediator in sepsis-induced ARDS.[6] LPS activates the nuclear factor-κB (NF-κB) signaling cascade via the Toll-like receptor 4 (TLR4) pathway, promoting the release of pro-inflammatory cytokines and contributing to multi-organ dysfunction, including the lungs, brain, kidneys, and liver.[7–9] Notably, dysregulated immune responses—especially macrophage-mediated cytokine release and NF-κB pathway activation—play a central role in ARDS pathogenesis and lung injury progression.[10,11] In experimental studies, intraperitoneal LPS administration is widely used to model extrapulmonary (indirect) ARDS, as it mimics systemic inflammation and leads to secondary lung injury without direct pulmonary insult.[12] This model closely reflects the pathophysiological features of sepsis-associated ARDS, which accounts for a significant portion of clinical cases. Recent studies have highlighted the significance of systemic immune regulation in the pathogenesis of ARDS.[13] Recent evidence emphasizes the importance of systemic immune regulation—including the roles of adipose tissue, bone marrow, and gut microbiota—in modulating ARDS progression through their effects on immune cell function and inflammatory responses.[14,15] Therefore, a deeper understanding of these systemic immune mechanisms may inform the development of targeted immunomodulatory therapies for ARDS.

Adipose tissue is a highly dynamic and metabolically active organ that plays fundamental roles in energy homeostasis, endocrine regulation, and immune modulation.[15,16] Adipose tissue comprises white, brown, and beige adipocytes.[17] White adipocytes primarily function to store energy and secrete adipokines,[18] while brown and beige adipocytes exhibit thermogenic capacity.[19] Notably, beige adipocytes can be induced by stimuli such as cold exposure or exercise.[20] Among the various white adipose tissue depots, subcutaneous adipose tissue (SAT) represents the largest depot, accounting for over 80% of total fat mass.[21,22] In contrast to visceral fat, SAT is more widely distributed and has garnered increasing attention for its immunomodulatory functions, particularly in pulmonary diseases.[23] Emerging evidence underscores its role in regulating systemic inflammation and maintaining immune homeostasis.[24–26] SAT mediates many of its effects through adipokines and extracellular vesicles (SAT-EVs), which are nanoscale vesicles (30–150 nm) carrying proteins, nucleic acids, and lipids. These vesicles facilitate intercellular communication and immune regulation.[27] Previous studies have demonstrated that adipose-derived EVs modulate lung inflammation and pulmonary fibrosis,[28,29] indicating their potential as therapeutic agents for ARDS. Nevertheless, the precise molecular mechanisms underlying these effects remain largely unexplored.

MicroRNAs (miRNAs) are among the most biologically active components of adipose-derived EVs. Changes in circulating or extracellular vesicle miRNA profiles are related to various pathological conditions, including tumors, infections, and metabolic diseases.[30,31] EV-derived miRNAs modulate the progression of ARDS by regulating gene expression in target tissues.[28] Recent studies have highlighted the therapeutic potential of miRNA-containing EVs in ARDS. For example, EVs from M2 macrophages can alleviate ARDS by delivering miR-709 to alveolar macrophages,[32] while bone marrow mesenchymal stem cell-derived EVs carrying miR-21-5p improve LPS-induced acute lung injury (ALI), an established model of ARDS.[33] Collectively, these findings underscore the role of EV-mediated miRNA transfer in modulating lung inflammation and highlight their potential as therapeutic agents for ARDS.

Although clinical interventions for ARDS are typically administered after disease onset, a pre-treatment model was employed in this study to investigate the early protective and mechanistic effects of SAT-EVs under controlled experimental conditions. This design facilitated the assessment of direct biological effects while minimizing variability due to disease progression, thereby providing a rational basis for future studies evaluating SAT-EVs as potential early-stage or preventive interventions for ARDS.

The findings of this study demonstrate that SAT-EV-derived miRNAs exert protective effects against ARDS by modulating the inflammatory response of pulmonary macrophages. The effects of SAT-EVs on ARDS were first evaluated in vivo, followed by in vitro and in vivo assessments of their regulatory roles in lung macrophage-mediated inflammation. In addition, miRNA profiling of SAT-EVs was performed to explore potential molecular mechanisms

underlying their immunomodulatory effects. By providing mechanistic insights into SAT-EV-mediated regulation of lung inflammation, this study advances the understanding of ARDS pathophysiology and proposes SAT-EVs as a promising therapeutic strategy for mitigating disease severity.

Materials and Methods

SAT-EVs Isolation, Characterization, and Treatment

EVs were isolated from subcutaneous adipose tissue (SAT) using differential ultracentrifugation. SAT was first cut into 1 mm^3 pieces and digested with a specific enzymatic solution at 37°C for 5 h with gentle shaking until a milky suspension was formed. The digestion was terminated using DMEM containing 10% exosome-depleted serum. The suspension underwent differential centrifugation at 2000×g, 4 °C for 5 min. Approximately 50 mL of supernatant was collected. A second centrifugation was performed at the same speed for 30 min to remove larger vesicles. The supernatant was filtered using a 0.45 μm membrane to collect the filtrate. Ultracentrifugation was conducted at low temperature (100,000×g for 70 min). The supernatant was discarded and the remaining pellet was resuspended in pre-chilled PBS (1× concentration). The resuspended samples were subjected to another round of ultracentrifugation under similar conditions for further purification. Finally, the resulting pellet containing sEVs was reconstituted in PBS and kept at a low temperature.[34] Western blotting was performed according to the guidelines of the International Society for Extracellular Vesicles (ISEV).[35] CD9, Alix, and Tsg101 were used as EV markers, while Calnexin served as a negative control to exclude contamination from cellular organelles. As EVs lack consistent cytoplasmic content, no universal loading control is currently available; therefore, marker profiling was used for qualitative validation rather than quantitative analysis. Nanoparticle tracking analysis (NTA) was performed using a NanoFCM-N30E to measure the size distribution of the particles based on light scattering and Brownian motion. The structure and morphology of the EVs were visualized using transmission electron microscopy (TEM, HITACHI, Japan). The protein concentration of the SAT-EVs was evaluated using a BCA protein assay kit.

Animals and Treatments

Ethical approval for the animal procedures was granted by the Animal Ethics Committee of University-Town Hospital, Chongqing Medical University. All animal experiments were conducted in accordance with the guidelines for the care and use of laboratory animals issued by the National Institutes of Health (NIH) and the Guiding Opinions on Treating Laboratory Animals Kindly (Document No. [2006]398), issued by the Ministry of Science and Technology of China on September 13, 2006. Male C57BL/6 mice were procured from Chongqing Enbi Biotechnology Co., Ltd. Healthy donor mice were anesthetized with 80 mg/kg ketamine, and a midline incision was made after thorough disinfection. Briefly, mice were placed in a supine position during the incision to expose and isolate the subcutaneous adipose tissue, where EVs were extracted via ultracentrifugation.

Sixty male C57BL/6 mice were randomly assigned to four groups: Sham, SAT-EVs, LPS, and SAT-EVs + LPS (n = 15 per group). Mice in the SAT-EVs and SAT-EVs + LPS groups were administered 1×10^9 particles of SAT-EVs via the tail vein under anesthesia, while mice in the Sham and LPS groups received an equal volume of sterile saline. To establish an extrapulmonary ARDS model, mice in the LPS and SAT-EVs + LPS groups were intraperitoneally injected with lipopolysaccharide (LPS, 15 mg/kg, *Escherichia coli* O55:B5; Sigma-Aldrich) 3 hours after the administration of SAT-EVs or saline. Mice were sacrificed 18 hours after LPS injection for sample collection and analysis. This model induces systemic inflammation without causing direct pulmonary injury and has been widely used to simulate sepsis-associated ARDS. Mice in the Sham and SAT-EVs groups received an equal volume of phosphate-buffered saline (PBS) via the intraperitoneal route.

To investigate the functional role of miR-26a-5p in ARDS, mice were treated with either a miR-26a-5p antagomir (a chemically modified antisense oligonucleotide that specifically inhibits miR-26a-5p) or an antagomir-NC (a non-targeting negative control oligonucleotide with no known complementarity to mouse miRNAs). Both reagents were obtained from Qiyunbio (China) and diluted in nuclease-free water. For in vivo inhibition, 20 nmol of antagomir or antagomir-NC was administered via tail vein injection once daily for three consecutive days prior to LPS and/or SAT-EVs treatment. Mice

were randomly assigned to four groups (n = 15 per group): LPS, SAT-EVs + LPS, LPS + SAT-EVs + antagomir-NC, and LPS + SAT-EVs + miR-26a-5p antagomir. At 18 hours post-LPS injection, mice were anesthetized, and blood samples were collected via orbital sinus puncture. Mice were subsequently euthanized by cervical dislocation in accordance with approved humane endpoints.

For survival analysis, an additional 36 mice were randomly divided into three groups (n = 12 per group): SAT-EVs, LPS, and SAT-EVs + LPS. Rectal temperatures were recorded every 12 hours for 120 hours. Mice with body temperatures below 30 °C were considered moribund and were euthanized. Furthermore, 24 mice were assigned to two groups (LPS + SAT-EVs + antagomir-NC and LPS + SAT-EVs + miR-26a-5p antagomir) for body temperature monitoring under the same protocol to assess the functional role of miR-26a-5p inhibition in vivo.

Lung Tissue Analysis

Lung tissues were collected 18 h after LPS injection. Lung lobes were perfusion-fixed with buffered formalin and embedded in paraffin. Tissue sections were stained with hematoxylin and eosin (H&E) and evaluated by a pathologist for pathological features. The severity of lung injury was quantitatively assessed using the modified Smith pathological scoring system, which evaluates pulmonary edema, alveolar and interstitial inflammation, alveolar and interstitial hemorrhage, and atelectasis. This scoring system employs a five-level grading scale ranging from 0 to 4, where 0 indicates normal lung morphology, 1 indicates mild injury, 2 indicates moderate injury, 3 indicates severe injury, and 4 indicates extremely severe injury.[36]

Mouse laryngeal tissue was dissected, and a needle was inserted into the exposed trachea and sutured. Lung lavage was performed by flushing the lungs twice with 500 μL of precooled PBS, recovering approximately 90% of the bronchoalveolar lavage fluid (BALF). The collected BALF was purified by centrifugation at 3000 rpm at 4 °C for 10 min. The protein concentration in the BALF was determined using a BCA protein assay kit (Beyotime).

In this study, the left lung tissue was collected from the mice after modeling, and the wet weight was measured. The tissues were then dried in a 65 °C incubator. Dry weight was measured after 24 h to calculate the wet-to-dry weight ratio.

ELISA Analysis and Myeloperoxidase (MPO) Activity

The levels of CCL2, IL-6, IL-1β, and TNF-α in BALF and cell supernatants were quantified using ELISA kits according to the manufacturer's guidelines (NeoBioscience Technology Co., China). MPO activity in 20 mg of lung tissue was evaluated using an MPO colorimetric activity assay kit (A044-1-1; Nanjing Jiancheng Bioengineering Institute).

Western Blotting (WB)

Lung tissues and cells were lysed in RIPA buffer (C500007, Sangon Biotech) containing PMSF (A610425, Sangon Biotech), followed by addition of 5X loading buffer (C506032, Sangon Biotech, China). The samples were boiled for 10 min at high temperature to ensure complete denaturation and dissociation and then separated by 10% SDS-PAGE. The proteins were blotted onto PVDF membranes after electrophoresis, and the membranes were blocked with a nonfat milk solution for 1 h to prevent nonspecific binding. The membranes were incubated overnight at 4 °C with primary antibodies to ensure optimal binding to target proteins, including Chuk (1:2000, ET1611-15, HUABIO, China), CD9 (1:500, ab307885, Abcam, China), IL-1β (1:1000, 31202T, CST, US), TSG101 (1:2000, ab125011, Abcam, China), Calnexin (1:1000, 66,903-1-IgG, MCE, China), GAPDH (1:1000, GB15004, Servicebio, China), iNOS (1:1000, 18,985-1-AP, Proteintech, China), Phospho-p65 (1:1000, 3033T, CST, US), p65 (1:1000, 8242T, CST, US), IκBα (1:1000, 4014T, CST, US), Phospho-IκBα (1:1000, 2859T, CST, US), and PTGS2 (1:1000, 12282T, CST, US). The membrane was then washed three times for 10 min each with TBST and shaking at 80–100 rpm. Next, the cells were incubated with the secondary antibodies for 2 h. Chemiluminescent reagents were used to visualize the protein bands.

Real-Time Polymerase Chain Reaction (RT-PCR)

TRIZOL Reagent (Takara Bio, Inc). was used for RNA extraction from the tissue and cellular samples, whereas TRIzol LS Reagent (Thermo Fisher Scientific, US) was used for RNA extraction from SAT-EVs. Reverse transcription was performed using a PCR reverse transcription kit (RR037A; Takara Bio, Inc). to convert 1 μg RNA into complementary

DNA (cDNA). MiRNA synthesis was performed using the stem-loop technique. qPCR was performed in a final reaction volume of 20 μL. Primers for mRNA and miRNA were obtained from Sangon Biotech, and ACTB (β-actin) or U6 was used as the internal reference. Details of the specific primer sequences are provided in Supplementary Table 1.

Cell Culture and Treatment

The murine macrophage cell line RAW264.7 (Meipunosai, China) was used to establish the in vitro inflammatory model of ARDS. This cell line was chosen for its stable macrophage phenotype, high responsiveness to LPS, and consistency with our murine in vivo ARDS model. Compared to PMA-induced THP-1-derived macrophages, RAW264.7 cells offer greater experimental reproducibility, species compatibility, and sensitivity to inflammatory stimuli, making them well-suited for modeling acute pulmonary inflammation. RAW 264.7 cells were grown in DMEM (Gibco, China) supplemented with 10% fetal bovine serum, 1% penicillin, and 1% streptomycin. LPS was diluted to the appropriate concentration using serum-free DMEM. The inhibitor-NC and miR-26a-5p inhibitors (provided by Guangzhou GeneCloud Biotechnology Co., Ltd). were dissolved in RNase-free water. The cells were assigned to different experimental groups based on their specific treatments as follows: the control group (no treatment), SAT-EVs group (treated with 1×10^8 particles/mL SAT-EVs), LPS group (exposed to 200 ng/mL LPS for 18 h), SAT-EVs + LPS group (pretreated with 1×10^8 particles/mL SAT-EVs for 6 h followed by 200 ng/mL LPS treatment for 18 h), SAT-EVs + LPS + inhibitor-NC group (treated with inhibitor-NC for 36 h, pretreated with 1×10^8 particles/mL SAT-EVs for 6 h, followed by 200 ng/mL LPS treatment for 18 h), and SAT-EVs + LPS + miR-26a-5p inhibitor group (treated with the miR-26a-5p inhibitor for 36 h, pretreated with 1×10^8 particles/mL SAT-EVs for 6 h, followed by 200 ng/mL LPS treatment for 18 h). The cells were incubated overnight to allow growth until they reached 60% confluence before drug treatment.

SAT-EVs Labeling and Tracking

SAT-EVs were mixed with 10 μM DiD staining reagent (Umibio, Shanghai, China), vortexed thoroughly, and incubated at 37°C for 1 h under light-shielding conditions. The labeled SAT-EVs were ultracentrifuged at 100,000 × g for 70 min to collect EVs as pellets. The pellet was then reconstituted in PBS for further use. The mice were injected with DiD-labeled SAT-EVs (60 μg) via the tail vein. In vivo imaging was conducted 3 and 6 h post-injection. PKH26-labeled SAT-EVs (15 μg) were incubated overnight with RAW 264.7 macrophages at 37°C, followed by a 5-minute counterstaining with DAPI. Samples were visualized using a fluorescence microscope, and high-resolution images were acquired to further analyze particle distribution and fusion within the cells. Five randomly selected areas per section were analyzed.

Small RNA and mRNA Sequencing

Total RNA was extracted from SAT-EVs for microRNA sequencing (miRNA-seq). Library preparation for miRNA-seq was performed by Xiamen Life Interconnect Technology Co., Ltd. Additionally, total RNA was extracted from si-CHUK–transfected cells (cells transfected with CHUK small interfering RNA) for mRNA sequencing, which was carried out by Guangzhou GenCloud Biotechnology Co., Ltd. All sequencing, including PCR product sequencing, was performed using the Illumina platform.

Dual-Luciferase Reporter Assay

The synthesized CHUK 3′-UTR was cloned into the pmirGLO3 vector (Qiyunbio, Guangzhou, China) based on predictions from the online tool miRWalk. The resulting CHUK 3′UTR-WT and CHUK 3′UTR-MUT reporter plasmids were co-transfected into 293T cells together with either a miR-26-5p mimic or a negative control mimic (mimic-NC). After 48 hours, the cells were harvested and lysed. Luciferase activity was measured using a Dual-Luciferase® Reporter Assay System (Promega, Madison, WI, USA).

Statistical Analysis

All experiments were conducted in triplicate to ensure accuracy and consistency. Statistical analyses were performed using GraphPad Prism software. The results are expressed as the mean ± standard deviation. The treatment and control

groups were compared using Student's *t*-test. Multiple group comparisons were performed using a one-way ANOVA. Statistical significance was set at $p < 0.05$.

Results

Characterization of SAT-EVs

A flowchart of the SAT-EV extraction process is presented in Figure 1A. SAT-EVs were isolated from white strip-like subcutaneous adipose tissue dissected from the abdominal region of mice (Figure 1B). Nanoparticle tracking analysis (NTA) indicated that most SAT-EVs measured 50–150 nm, with a peak diameter of 75.5 nm, and a particle concentration of approximately 8.46×10^8 particles/mL (Figure 1C). The SAT-EVs exhibited a characteristic bilayer membrane structure and appeared round or cup-shaped under TEM (Figure 1D). Additionally, SAT-EVs highly expressed Alix,

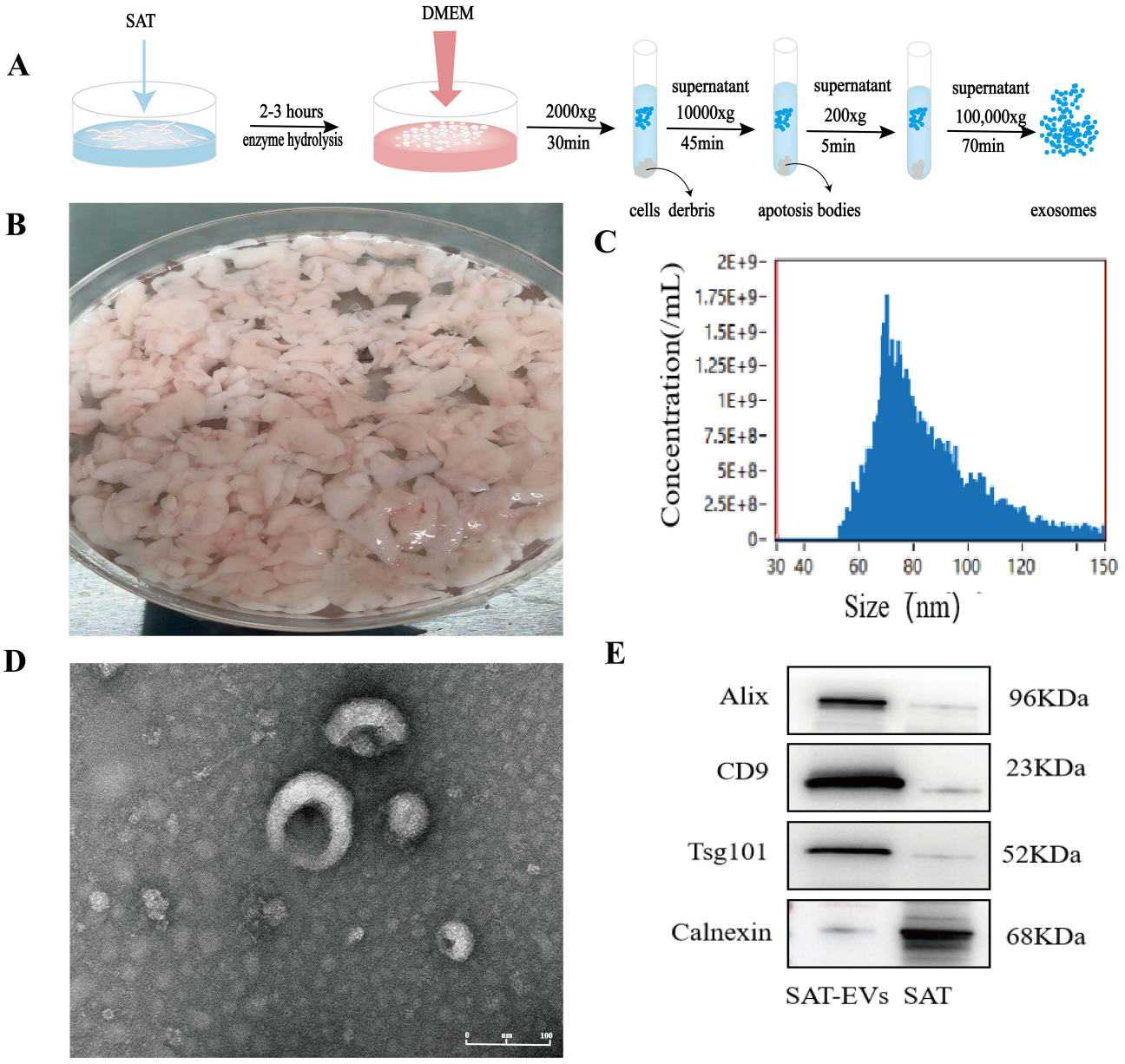

Figure 1 Characterization of SAT and SAT-EVs. (**A**) Schematic illustration of SAT-EVs extraction. (**B**) Subcutaneous adipose tissue was isolated from the abdominal region of mice. (**C**) NTA of SAT-EVs showing the size distribution and concentration. (**D**) TEM visualization showing the morphology of SAT-EVs (Scale bar = 100 nm). (**E**) WB analysis of SAT-EVs and SAT showing EV markers (Alix, CD9, Tsg101) and negative marker (Calnexin).

CD9, and Tsg101 but lacked the expression of calnexin, an endoplasmic reticulum marker protein commonly found in adipose tissue (Figure 1E). Collectively, these results confirm that the isolated SAT-EVs meet the criteria for exosome morphology, concentration, size distribution, and protein markers, indicating high purity.

SAT-EVs were Internalized by Lung Tissue and Improved Survival in ARDS Mice

C57BL/6J mice were used to establish an ARDS model via intraperitoneal injection of LPS, as previously described, to investigate the potential therapeutic effects of SAT-EVs.[37] The experimental protocol applied is shown in Figure 2A. DiD-labeled SAT-EVs were injected via the tail vein to confirm whether SAT-EVs could enter mouse lung tissue. In vivo imaging was conducted at 3 and 6 h post-injection. DiD-labeled SAT-EVs were detected in the mouse lung tissue at 3 h,

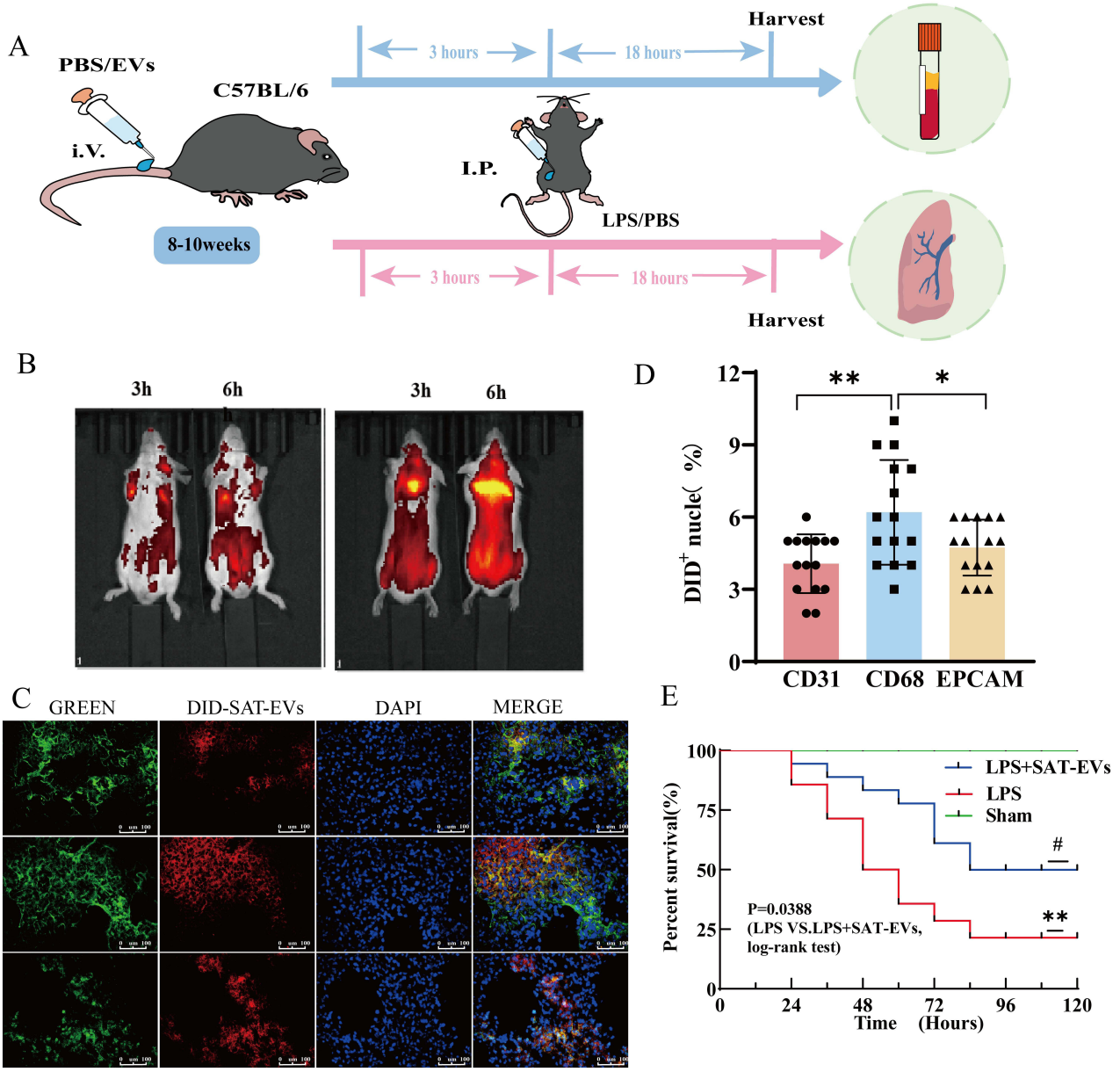

Figure 2 SAT-EVs in a mouse model of ARDS. (**A**) Schematic illustration of SAT-EVs administration in ARDS mice. (**B**) DID-labeled SAT-EVs were imaged in mouse lung tissue. (**C**) Representative immunofluorescence images of CD31, CD68, and EPCAM in mouse lung tissue (n = 5 per group). (**D**) Quantification of Dil-labeled SAT-EVs in mouse lung tissue, showing uptake by three types of lung cells: CD31 (endothelial cells), CD68 (macrophages), and EPCAM (epithelial cells). n = 5 per group. $^{**}p < 0.01$ (CD31 vs CD68), $^{*}p < 0.05$ (CD68 vs EPCAM). (**E**) Kaplan–Meier survival analysis demonstrating significant differences among groups (n = 12 per group; Log rank test). **p < 0.01 (Sham vs LPS), #p < 0.05 (LPS vs LPS + SAT-EVs).

https://doi.org/10.2147/IJN.S514623

with fluorescence signals significantly increasing at 6 h (Figure 2B). Therefore, SAT-EVs were pre-administered 6 h before LPS treatment. The distribution of DiD-labeled SAT-EVs was observed in pulmonary macrophages, epithelial cells, and capillary endothelial cells (Figure 2C). The SAT-EV fluorescence intensity was markedly elevated in CD68-positive macrophages compared to that in CD31-positive endothelial cells and EPCAM-positive epithelial cells (Figure 2D). These results indicate that SAT-EVs can efficiently enter lung tissue and predominantly accumulate in pulmonary macrophages. Kaplan-Meier survival analysis revealed that the survival rate in the LPS group sharply decreased to approximately 25% within the first 48 h and was almost zero at 120 h. In contrast, the sham group maintained a stable survival rate of 100%, with no mortality. The survival rate in the LPS+SAT-EVs group gradually decreased from 100% to approximately 50% within the first 72 h. The survival rates differed significantly between the LPS+SAT-EVs and LPS groups, indicating that SAT-EVs effectively protected mice from LPS-induced mortality in the ARDS model ($p = 0.0388$, Log rank test) (Figure 2E).

SAT-EV Treatment Alleviates Lung Injury, Reduces Vascular Permeability, and Attenuates Inflammation in ARDS Mice

Pathological examinations were conducted to assess the effects of the SAT-EVs on tissue damage and inflammation. Lung tissues from LPS-treated mice exhibited pronounced alveolar septal thickening, abundant erythrocytes within the pulmonary vasculature, and exudates in the bronchi. These pathological alterations impaired gas exchange, a hallmark of ARDS. In contrast, co-treatment with SAT-EVs significantly alleviated inflammatory cell infiltration and preserved alveolar structure (Figure 3A). H&E-stained lung injury scores were higher in the LPS group than in the sham group, whereas SAT-EV treatment markedly reduced these scores (Figure 3B). LPS administration also led to a significant increase in total protein levels in BALF and in the lung wet-to-dry weight ratio. Both indices were significantly reversed following SAT-EV treatment (Figure 3C and D), indicating reduced pulmonary vascular permeability. Furthermore, SAT-EV treatment decreased LPS-induced elevation of MPO levels in lung tissue (Figure 3E). Analysis of inflammatory factors in BALF showed that the concentrations of TNF-α, IL-1β, IL-6, and CCL2 were markedly increased in the LPS group, but significantly attenuated after SAT-EV administration (Figure 3F–I). SAT-EVs also suppressed the LPS-induced upregulation of pro-inflammatory cytokine mRNA expression in lung tissue (Figure 3J–M). Immunohistochemical staining further confirmed these findings, revealing elevated expression of IL-6, IL-1β, TNF-α, and CCL2 in the lung tissues of LPS-treated mice. These increases were markedly reduced following SAT-EV treatment, highlighting an anti-inflammatory effect at the tissue level (Supplementary Figure S1). Collectively, these results indicate that SAT-EVs exert protective effects in ARDS mice by alleviating lung injury, reducing vascular permeability, and suppressing inflammatory responses.

SAT-EVs Mitigate LPS-Triggered Inflammation in RAW 264.7 Cells

Alveolar macrophages constitute approximately 55% of pulmonary immune cells and play a pivotal role in maintaining immune homeostasis during lung inflammation, including ARDS.[38] In this study, fluorescent labeling revealed that SAT-EVs predominantly accumulated in pulmonary macrophages (Figure 2C and D). Based on this observation, RAW 264.7 cells were selected for subsequent in vitro experiments. The experimental protocol for SAT-EV treatment in LPS-stimulated cells is illustrated in Figure 4A. To evaluate the uptake efficiency of SAT-EVs by macrophages, the vesicles were labeled with PKH26. Red fluorescence was observed in RAW 264.7 cells under a fluorescence microscope 6 h post-incubation, indicating successful internalization of SAT-EVs (Figure 4B). To mimic an inflammatory environment in vitro, cells were pretreated with SAT-EVs (1×10^8 particles/mL) for 6 h, followed by LPS stimulation for 18 hours. ELISA results showed that the concentrations of TNF-α, IL-1β, IL-6, and CCL2 in the cell supernatants were significantly elevated in the LPS group. However, SAT-EV pretreatment markedly reduced the levels of these inflammatory cytokines (Figure 4C-F). Furthermore, qPCR analysis revealed that the mRNA expression levels of TNF-α, IL-1β, IL-6, and CCL2 were significantly upregulated after LPS stimulation. SAT-EVs intervention markedly reduced the expression of these inflammatory genes (Figure 4G-J). These findings further confirm that SAT-EVs effectively suppress LPS-induced inflammatory responses in RAW 264.7 macrophages.

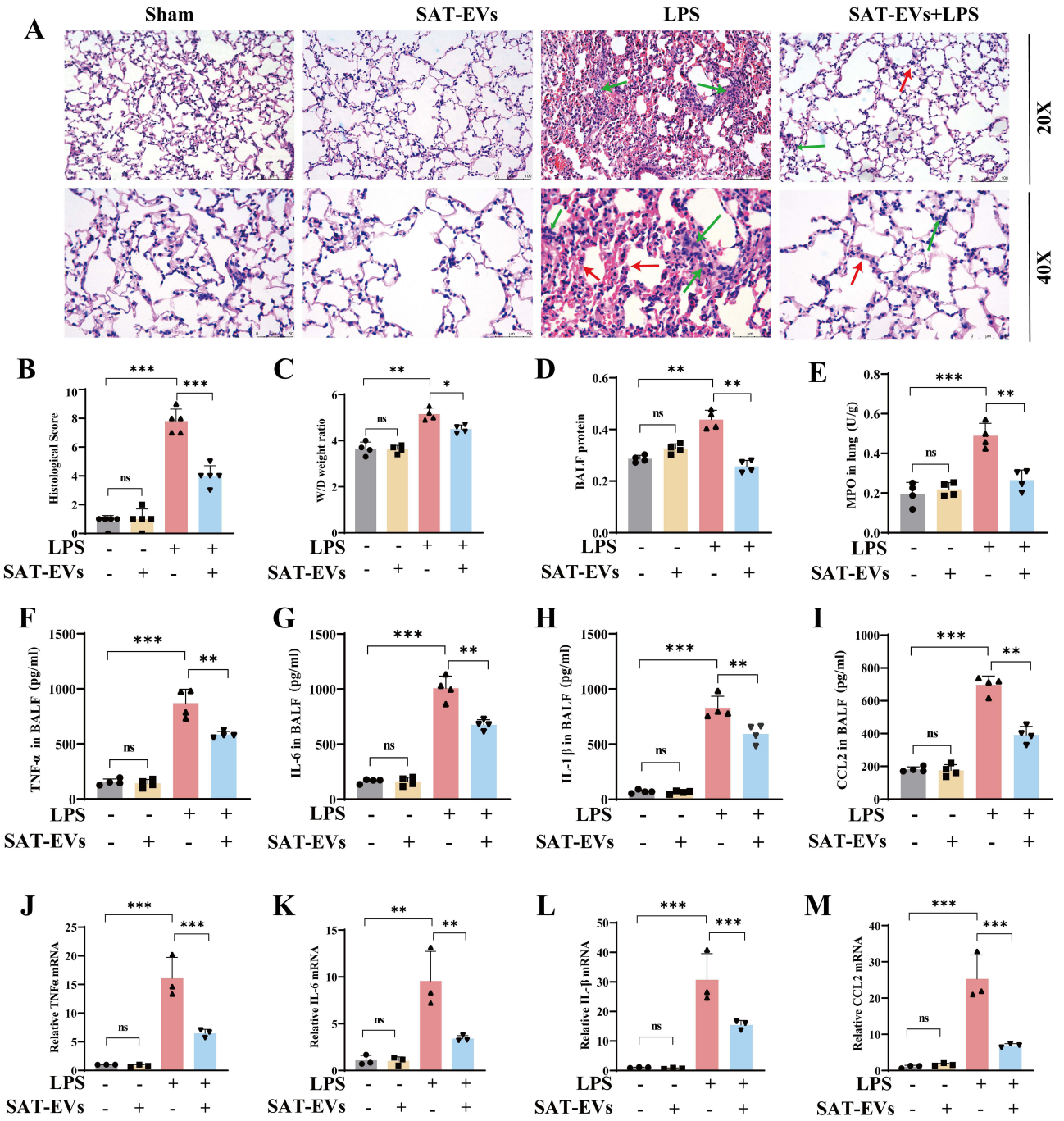

Figure 3 SAT-EVs alleviate lung injury and inflammation in LPS-induced ARDS mice. (**A**) Histological changes in lung tissue were assessed by H&E staining at ×200 and ×400 magnification.Green arrows highlight inflammatory cell infiltration, while red arrows indicate alveolar septal thickening. (**B**) Lung injury scores in different groups (n = 5). (**C**) Lung wet-to-dry weight ratio (n = 4). (**D**) Total protein concentration in BALF (n = 4). (**E**) MPO activity in lung tissue (n = 4). (**F–I**) Concentrations of TNF-α, IL-6, IL-1β, and CCL2 in BALF were measured by ELISA (n = 3–4). (**J–M**) mRNA expression levels of TNF-α, IL-6, IL-1β, and CCL2 in lung tissue were determined by qPCR (n = 3). *P < 0.05, **p < 0.01, ***p < 0.001.

SAT-EVs miR-26a-5p Modulates the CHUK/NF-κB Pathway

Adipose tissue is a major source of circulating exosomal miRNAs, which play a key role in intercellular communication.[39] In this study, transcriptome sequencing was performed on SAT-EVs to explore the potential molecular mechanisms by which they alleviate inflammatory responses in ARDS. KEGG pathway enrichment analysis based on miRNA expression levels revealed that the predicted target genes were primarily involved in pathways related to fatty acid metabolism, pathogen infection, and inflammation regulation (Supplementary Figures S2 and S3). Nine highly

https://doi.org/10.2147/IJN.S514623

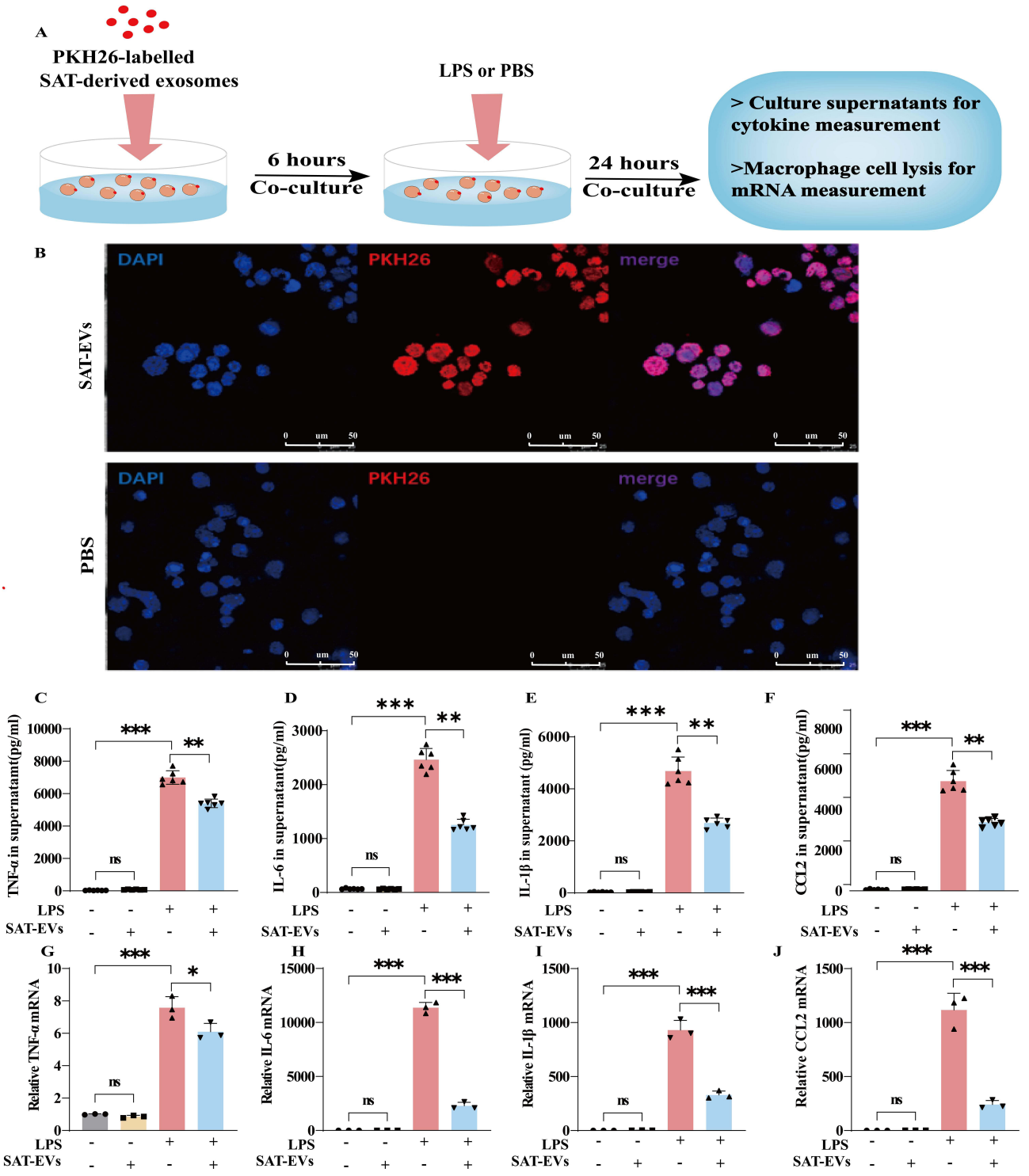

Figure 4 SAT-EVs suppress LPS-induced inflammation in RAW 264.7 cells. (**A**) Schematic of the experimental workflow for SAT-EV treatment. (**B**) Uptake of PKH26-labeled SAT-EVs by RAW 264.7 cells. (**C–F**) Protein levels of TNF-α, IL-6, IL-1β, and CCL2 in cell supernatants measured by ELISA (n = 3). (**G–J**) Relative mRNA expression of TNF-α, IL-6, IL-1β, and CCL2 analyzed by qPCR (n = 3). $^{**}p < 0.01$, $^{***}p < 0.001$.

expressed miRNAs were identified in SAT-EVs, including let-7a-5p, let-7c-5p, let-7d-5p, miR-191-5p, miR-2137, miR-26a-5p, miR-26b-5p, miR-5126, and miR-30d-5p. Among these, RT-PCR analysis confirmed that miR-26a-5p expression was significantly elevated in SAT-EVs (Figure 5A). miR-26a-5p is an evolutionarily conserved miRNA known to exert anti-inflammatory effects in both humans and mice (Figure 5B).

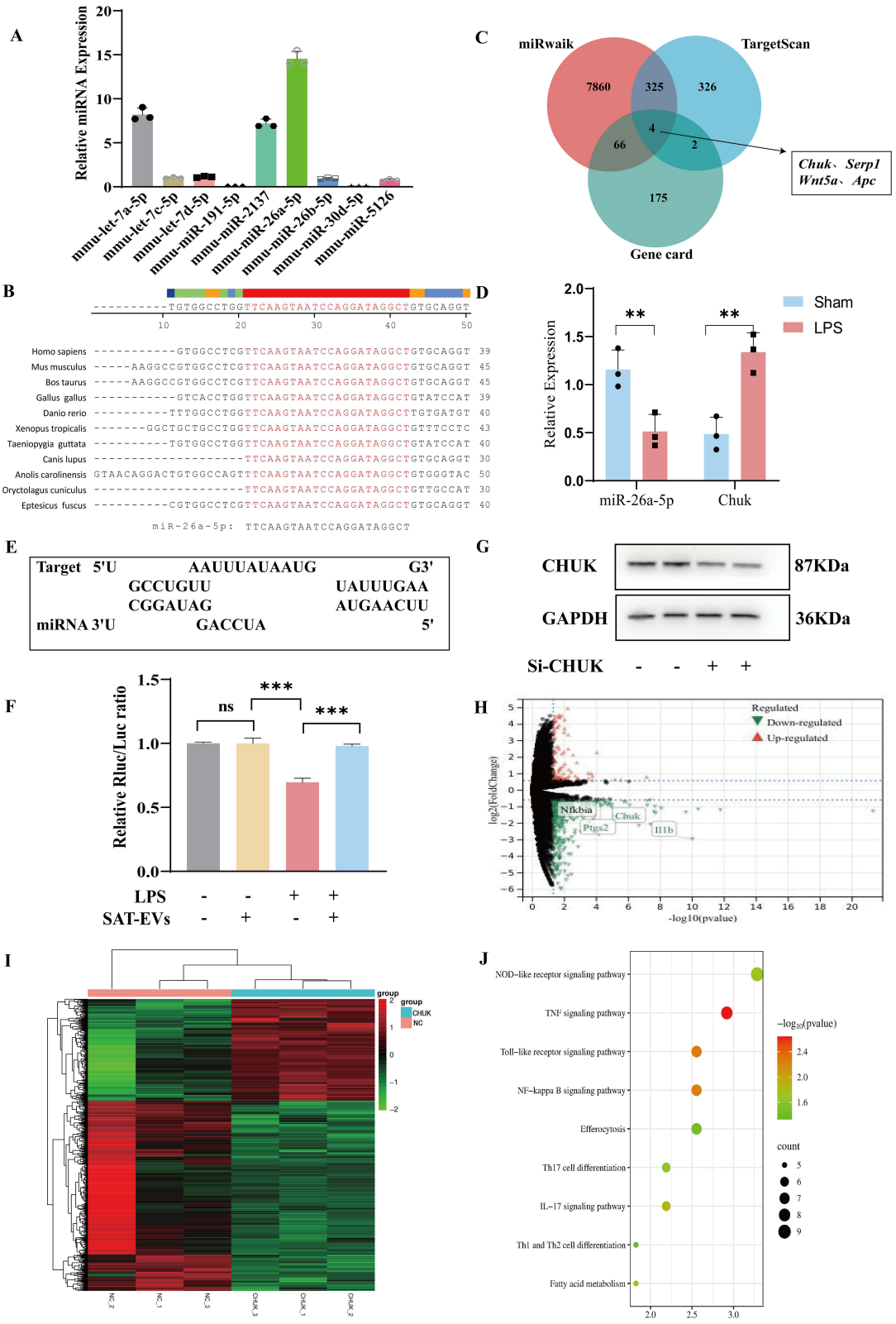

Figure 5 miR-26a-5p is enriched in SAT-EVs and targets *Chuk* to regulate the NF-κB signaling pathway. (**A**) Relative expression level of miR-26a-5p in SAT-EVs determined by qRT-PCR. (**B**) Evolutionary conservation of miR-26a-5p across species. (**C**) Venn diagram showing the overlap between predicted miR-26a-5p target genes and ARDS-related genes. (**D**) Relative expression analysis of miR-26a-5p and *Chuk*. (**E**) Predicted binding site between miR-26a-5p and the 3′UTR of Chuk. (**F**) Dual-luciferase reporter assay confirming direct targeting of Chuk by miR-26a-5p (n = 5; **p < 0.01). (**H**) CHUK protein levels following siRNA-mediated knockdown. (**G**) Western blot analysis of CHUK expression following siRNA-mediated knockdown. (**H** and **I**) Volcano plot and heatmap showing differentially expressed genes between si-Chuk and si-control groups. (**J**) KEGG pathway analysis showing enrichment of NF-κB signaling–related genes among DEGs.

https://doi.org/10.2147/IJN.S514623

Potential gene targets of miR-26a-5p were predicted using the miRWalk and TargetScan databases. These results were cross-referenced with genes associated with "sepsis-associated lung injury" in the GeneCards database. Intersection analysis identified four candidate target genes: *Serp1, Chuk, Wnt5a*, and *Apc* (Figure 5C). The expression levels of miR-26a-5p and these candidate genes were measured in mouse lung tissue, followed by correlation analysis. Notably, miR-26a-5p expression was inversely correlated with *Chuk* expression, suggesting a potential regulatory relationship (Figure 5D). miR-26a-5p exhibits partial complementarity with the 3′ untranslated region (3′UTR) of Chuk mRNA, particularly within the seed region (nucleotides 2–8 from the 5′ end of the miRNA), suggesting a potential post-transcriptional regulatory interaction (Figure 5E). To validate the predicted interaction, a dual-luciferase reporter assay was performed. Co-transfection of miR-26a-5p with a reporter construct containing the wild-type Chuk 3′UTR (3′UTR-WT) resulted in a significant decrease in luciferase activity, whereas no such effect was observed with the mutant construct (3′UTR-MUT) (Figure 5F). These results demonstrate that miR-26a-5p directly targets CHUK, a key component of the IκB kinase (IKK) complex.

To investigate the underlying molecular mechanisms, siRNA-mediated knockdown of *Chuk* was performed (Figure 5G), followed by transcriptome sequencing of si-Chuk samples. Differential expression analysis identified 1120 mRNAs in the si-Chuk group, including 402 upregulated and 718 downregulated transcripts (Figure 5H). A heatmap was generated to visualize the clustering of these differentially expressed genes (DEGs) (Figure 5I). KEGG pathway analysis revealed that the DEGs were primarily enriched in inflammation-related pathways, including cytokine–cytokine receptor interactions, TNF signaling, NF-κB signaling (involving *Ikbα, Chuk, Parp1, Il1b, Tnfaip3, Ptgs2*, and *Bcl2a1*), and NOD-like receptor signaling (Figure 5J). CHUK is a key component of the IκB kinase (IKK) complex. It facilitates phosphorylation-dependent degradation of IκB proteins, leading to the release and nuclear translocation of NF-κB, which subsequently triggers the transcription of inflammatory genes. These findings suggest that miR-26a-5p, delivered via SAT-EVs, exerts protective effects in ARDS by modulating the CHUK/NF-κB signaling pathway.

SAT-EVs Alleviate ARDS Inflammation by Modulating miR-26a-5p/CHUK/NF-κB Signaling in vitro and in vivo

Compared with the untreated control, SAT-EVs treatment significantly upregulated miR-26a-5p expression in RAW 264.7 cells in vitro (Figure 6A). Additionally, pretreatment with SAT-EVs markedly reduced CHUK protein expression levels. WB analysis demonstrated significantly increased levels of NF-κB pathway-related proteins (IκB-α, p-IκB-α, P65, p-P65) and inflammation-related proteins (iNOS, IL-1β, and PTGS2) following LPS stimulation. These elevations were effectively reversed by SAT-EVs treatment (Figure 6B–D).

In vivo, miR-26a-5p expression significantly decreased in lung tissues after LPS exposure compared to the normal control. However, SAT-EVs treatment restored miR-26a-5p levels significantly (Figure 6E). Consistently, SAT-EVs reduced CHUK protein levels in the lung tissues of LPS-treated mice (Figure 6F). These findings suggest that SAT-EVs effectively deliver miR-26a-5p to recipient cells, thereby modulating CHUK expression. Further in vivo WB analysis confirmed elevated expression of NF-κB-related proteins (IκB-α, p-IκB-α, P65, p-P65) and inflammatory proteins (iNOS, IL-1β, PTGS2) following LPS stimulation. SAT-EVs treatment significantly reversed these increases (Figure 6G and H). Immunofluorescence staining further validated the ability of SAT-EVs to reduce LPS-induced upregulation of iNOS, IL-1β, and PTGS2 in lung tissues of ARDS mice (Figure 6I).

Collectively, these results demonstrate that SAT-EVs deliver miR-26a-5p to alveolar macrophages, inhibit the CHUK/NF-κB signaling pathway, and subsequently reduce organ-specific inflammation, ultimately alleviating ARDS.

miR-26a-5p Inhibition Diminishes the Anti-inflammatory Effects of SAT-EVs on LPS-triggered Inflammation in RAW 264.7 Cells

To investigate whether the anti-inflammatory effects of SAT-EVs are mediated by miR-26a-5p, miR-26a-5p expression was silenced using a specific miRNA inhibitor. The inhibitor was co-transfected with RAW 264.7 cells for 36 h. RT-PCR analysis confirmed that miR-26a-5p expression was significantly suppressed following transfection (Supplementary Figure S4). In LPS-stimulated macrophages, miR-26a-5p inhibition reversed the SAT-EV-induced reductions in TNF-α, IL-1β, IL-6, and CCL2 at both the mRNA and protein levels (Figure 7A–H). Moreover, qRT-PCR analysis confirmed

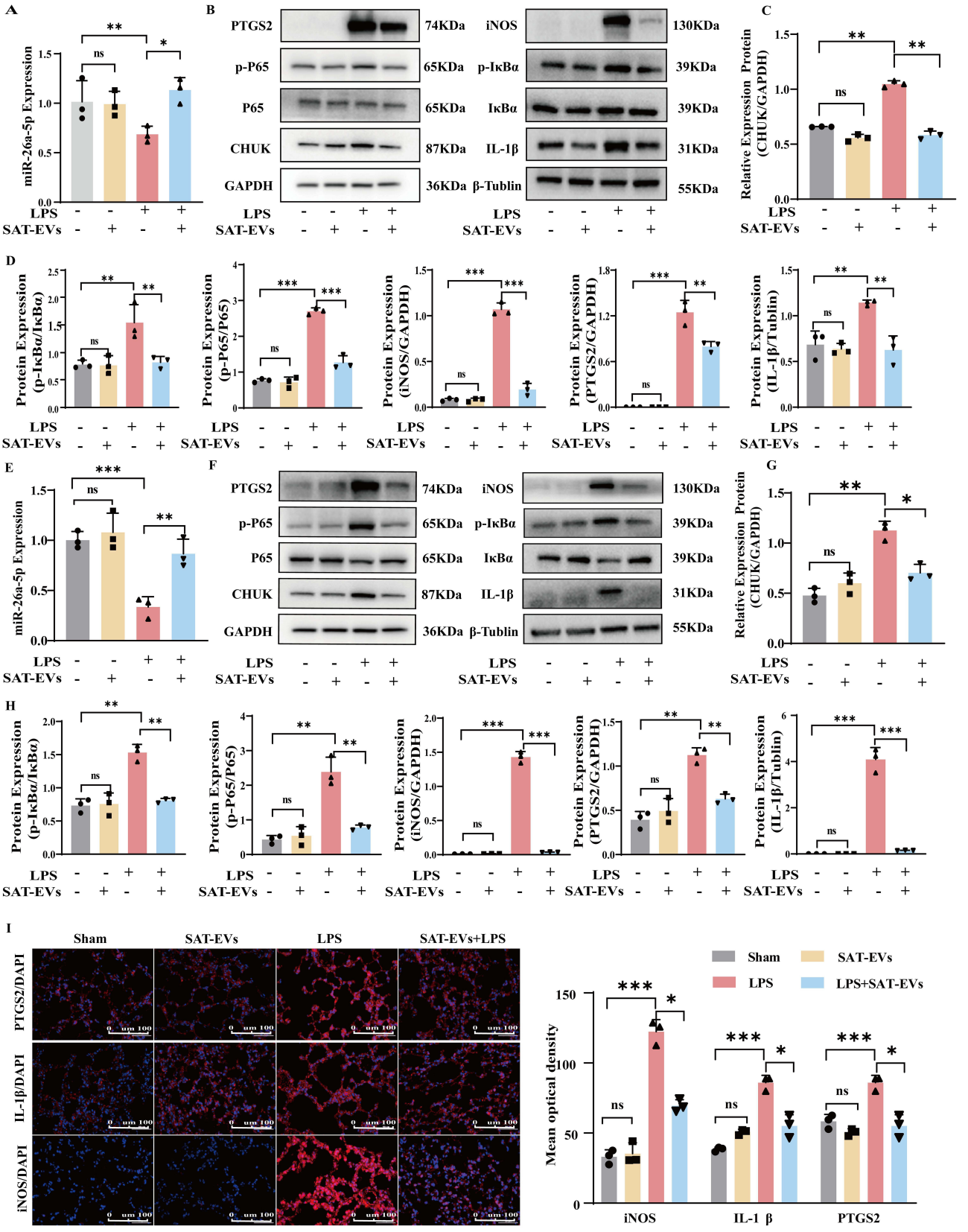

Figure 6 SAT-EVs modulate the CHUK/NF-κB signaling pathway in vitro and in vivo. (**A**) miR-26a-5p expression in RAW 264.7 cells following LPS and/or SAT-EV treatment. (**B**–**D**) Western blot analysis of CHUK, IκB-α, p-IκB-α, p65, p-p65, iNOS, IL-1β, and PTGS2 in RAW 264.7 cells. (**E**) miR-26a-5p expression in lung tissues from each experimental group. (**F–H**) Protein expression of CHUK/NF-κB signaling–related molecules and inflammatory markers in lung tissues. (**I**) Immunofluorescence staining of iNOS, IL-1β, and PTGS2 in lung tissue sections. n = 3 per group. $^{**}p < 0.01$, $^{***}p < 0.001$.

https://doi.org/10.2147/IJN.S514623

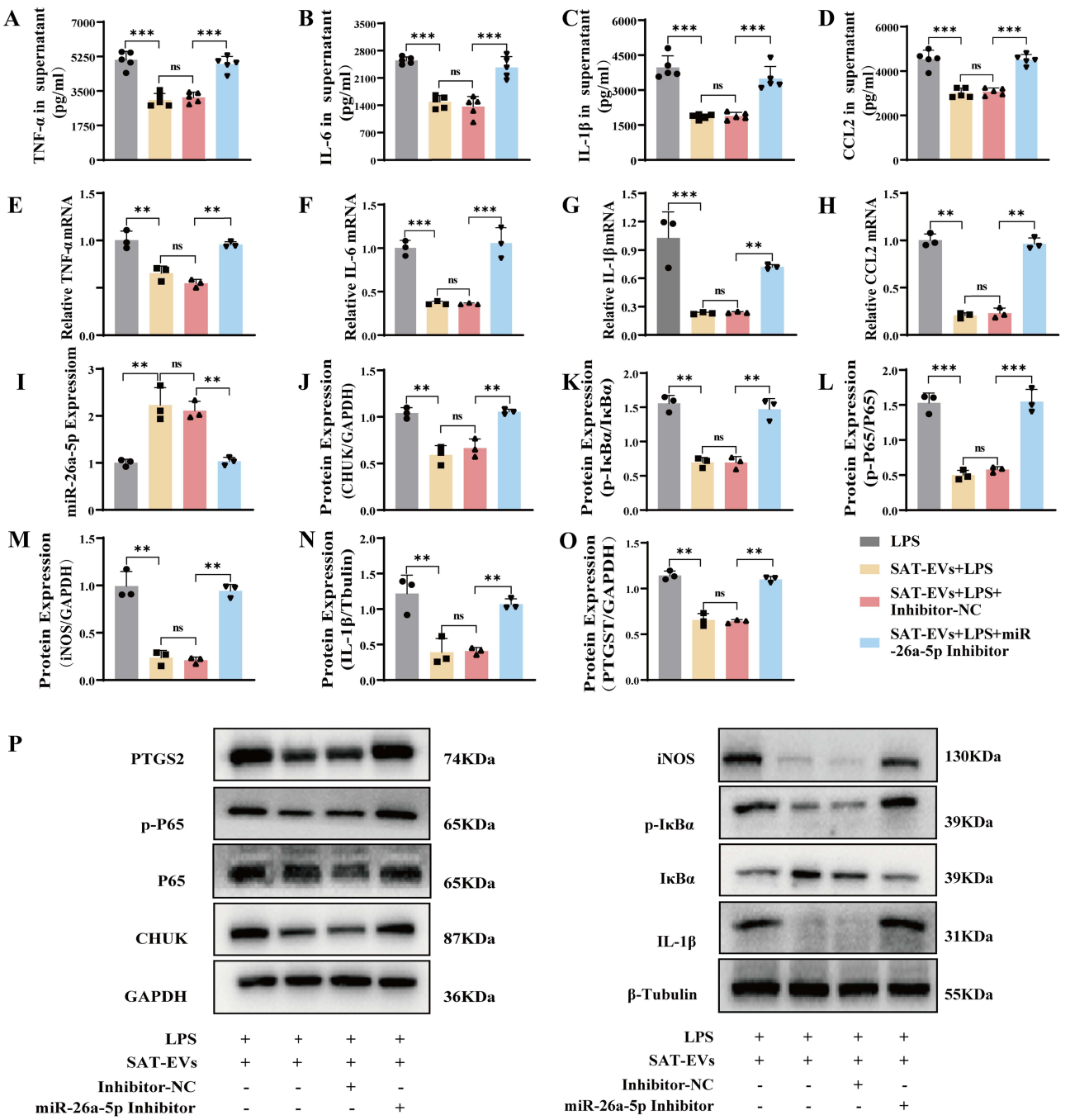

Figure 7 Inhibition of miR-26a-5p abolishes the anti-inflammatory effects of SAT-EVs in LPS-stimulated RAW 264.7 cells. (**A–D**) ELISA analysis of TNF-α, IL-6, IL-1β, and CCL2 protein levels in cell supernatants. (**E–H**) Relative mRNA expression of TNF-α, IL-6, IL-1β, and CCL2 in cells. (**I**) miR-26a-5p expression following inhibitor transfection. (**J–P**) Western blot analysis of CHUK, IκB-α, p-IκB-α, p65, p-p65, iNOS, IL-1β, and PTGS2 in cells treated with LPS, SAT-EVs, and/or miR-26a-5p inhibitor. n = 3–5 per group. $^{**}p < 0.01$, $^{***}p < 0.001$.

that SAT-EVs markedly upregulated miR-26a-5p expression, which was effectively reversed upon transfection with a specific miR-26a-5p inhibitor (Figure 7I). Consistently, the suppressive effects of SAT-EVs on the protein levels of CHUK, IκB-α, p-IκB-α, P65, p-P65, iNOS, IL-1β, and PTGS2 were abolished following miR-26a-5p knockdown (Figure 7J–P). These findings collectively suggest that the anti-inflammatory effects of SAT-EVs are, at least in part, mediated via the upregulation of miR-26a-5p.

Inhibition of miR-26a-5p Compromises the Protective Effects of SAT-EVs in ARDS Mice

In vivo, a miR-26a-5p antagomir was administered via tail vein injection for three consecutive days, followed by intravenous injection of 1×10^9 SAT-EV particles. Three hours later, a sepsis-related ARDS model was established by intraperitoneal injection of LPS. Survival analysis revealed a significant reduction in survival in the SAT-EVs + LPS + miR-26a-5p antagomir group compared with the SAT-EVs + LPS + antagomir-NC group (50% vs 70%, respectively; Figure 8A), indicating that miR-26a-5p inhibition impaired the survival benefit conferred by SAT-EVs. Histopathological evaluation further demonstrated that miR-26a-5p inhibition attenuated SAT-EVs-mediated lung protection, as indicated by increased lung injury scores (Figure 8B and C). In addition, SAT-EV treatment significantly reduced the lung wet/dry weight ratio and total protein concentration in BALF, whereas these improvements were reversed by the miR-26a-5p antagomir (Figure 8D and E). Consistently, lung MPO activity was elevated following miR-26a-5p antagomir (Figure 8F). Moreover, miR-26a-5p inhibition abolished the anti-inflammatory effects of SAT-EVs, Both mRNA and protein levels of TNF-α, IL-1β, IL-6, and CCL2 were significantly increased in the SAT-EVs + LPS + miR-26a-5p antagomir group compared with the SAT-EVs + LPS and SAT-EVs + LPS + antagomir-NC groups (Figure 8G–N). Consistent with these findings, immunohistochemical staining of lung tissues showed elevated expression of TNF-α, IL-1β, IL-6, and CCL2 in the antagomir-treated group, confirming the reversal of SAT-EV-induced anti-inflammatory effects (Supplementary Figure S5). Further supporting the loss of SAT-EV-induced anti-inflammatory effects. In parallel, the SAT-EV-induced upregulation of miR-26a-5p in LPS-treated lungs was significantly suppressed by the antagomir (Figure 8O). WB analysis confirmed that SAT-EV-mediated downregulation of CHUK, IκB-α, p-IκB-α, P65, p-P65, iNOS, IL-1β, and PTGS2 was reversed by miR-26a-5p inhibition (Figure 8P and Q). Immunofluorescence staining further demonstrated that the reduced expression of iNOS, IL-1β, and PTGS2 in response to SAT-EV treatment was abolished by the antagomir (Figure 8R). Collectively, these results indicate that the therapeutic effects of SAT-EVs in ARDS are, at least in part, mediated by miR-26a-5p-dependent regulation of the NF-κB signaling pathway.

Discussion

In this study, we demonstrated that SAT-EVs exert protective effects against ARDS, primarily by modulating the pulmonary macrophage inflammatory response. Mechanistically, SAT-EVs deliver miR-26a-5p to alveolar macrophages, thereby regulating the CHUK/NF-κB signaling pathway and mitigating ARDS-related inflammation.

Adipose tissue, as an active immune organ, exhibits complex and multidimensional immunomodulatory functions.[40] In addition to serving as an energy reserve, adipose tissue is essential to the immune system. Adipose tissue, particularly subcutaneous adipose tissue (SAT), is rich in a large number of immune cells, including innate immune cells (eg, macrophages, neutrophils, eosinophils, and natural killer cells) and adaptive immune cells (eg, T cells and B cells).[41] Adipocytes are central to the formation of the immune microenvironment; they not only participate in the metabolic function of adipose tissue but also play a key role in regulating systemic immune responses.[41–43] By directly or indirectly modulating the immune response of other tissues and organs through the secretion of various bioactive molecules, including cytokines, adipokines, and chemokines. Some studies have demonstrated the immunomodulatory role of chest adipose tissue in respiratory viral infections.[44] Additionally, adipose-derived leptin has been reported to modulate cellular and humoral immune responses and play an immunosuppressive role in a hamster model.[45] Adipose tissue and the macrophages within it also serve as a vital factor in the immune regulation of COVID-19.[46] Therefore, the potential role of adipose tissue in diseases related to immune dysregulation, particularly ARDS, warrants further investigation. By modulating the immune response, adipose tissue may offer new therapeutic strategies for correcting the immune imbalance in ARDS.

Adipose tissue is an important source of circulating EVs carrying functional miRNAs which have been shown to protect against ARDS.[47,48] Therefore, miRNA sequencing was performed on SAT-EVs to identify their functional molecules and mechanisms in ARDS. Several miRNAs, including let-7a-5p, let-7d-5p, miR-2137, miR-26a-5p, and miR-5126, were enriched in the SAT-EVs. These miRNAs can contribute to the repair of lung and other organ injuries. For instance, EVs carrying engineered let-7a-5p have been reported to alleviate LPS-induced ARDS.[49] Let-7d-5p was demonstrated to alleviate inflammation and apoptosis in rat intestinal epithelial cells,[50] and miR-2137 was implicated in

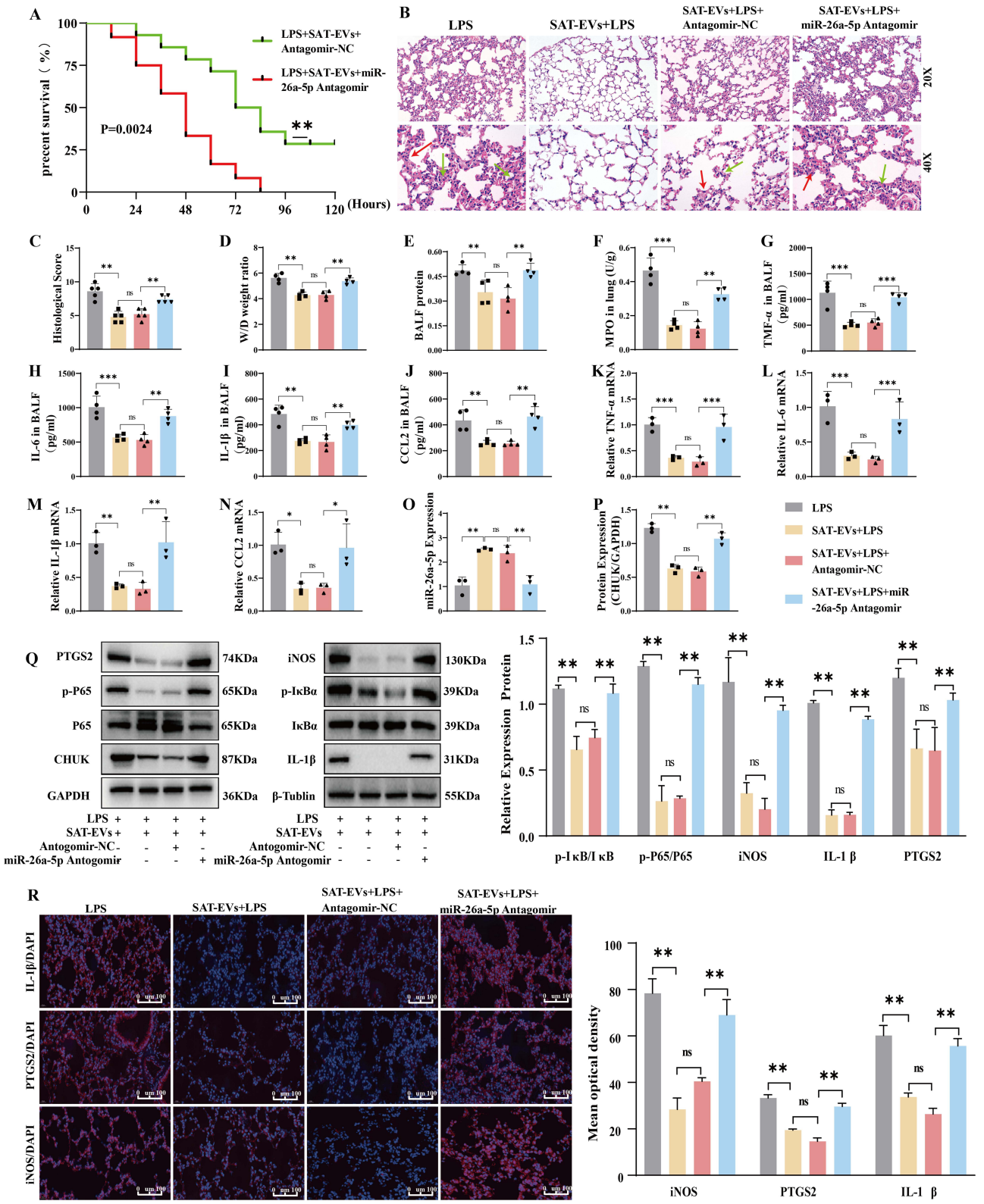

Figure 8 The protective effects of SAT-EVs in ARDS mice are dependent on miR-26a-5p. (**A**) Kaplan–Meier survival analysis of ARDS mice treated with SAT-EVs and/or miR-26a-5p antagomir (n = 12). (**B** and **C**) Representative H&E staining and lung injury scores, Green arrows highlight inflammatory cell infiltration, while red arrows indicate alveolar septal thickening. (**D–F**) Lung wet/dry ratio, BALF total protein, and MPO activity concentration. (**G–J**) BALF concentrations of TNF-α, IL-6, IL-1β, and CCL2 measured by ELISA. (**K–N**) mRNA expression levels of TNF-α, IL-6, IL-1β, and CCL2 assessed by qPCR. (**O**) miR-26a-5p expression in lung tissue. (**P** and **Q**) Western blot analysis of CHUK, IκB-α, p-IκB-α, p65, p-p65, iNOS, IL-1β, and PTGS2. (**R**) Immunofluorescence staining of iNOS, IL-1β, and PTGS2 in lung tissues. n = 3 per group unless otherwise specified. $^{**}p < 0.01$, $^{***}p < 0.001$.

the repair of acetaminophen-induced liver injury.[51] The miR-26a-5p can mitigate drug-induced liver injury[52] and myocardial ischemia-reperfusion injury.[53] Additionally, PCR analysis of the genes enriched in SAT-EV sequencing showed that the level of miR-26a-5p was the highest.

miR-26a-5p is a multifunctional miRNA with multiple functions in vivo. It modulates the progression of multiple cancers,[54,55] directly targets ACSL3 in adipocytes to regulate adipocyte differentiation,[56] participates in various cardiovascular diseases[57] and diabetic retinopathy.[58] Our results also demonstrate that SAT-EVs could deliver miR-26a-5p to macrophages in ARDS. SAT-EV treatment significantly upregulated miR-26a-5p levels in vitro and in vivo, while reducing LPS-induced elevation of inflammatory factors, such as TNF-α, IL-1β, IL-6, iNOS, PTGS2, and MCP-1. Knockdown of miR-26a-5p weakened or abolished the reduction in inflammatory factors and chemokines induced by SAT-EVs. Related studies have shown that miR-26a-5p alleviates sepsis-induced kidney injury[59] and atherosclerosis[60] by interacting with the NF-κB axis. Resveratrol inhibited apoptosis of umbilical vein endothelial cells by increasing miR-26a-5p levels.[61] Moreover, miR-26a-5p can prevent cellular injury and apoptosis associated with ischemia-reperfusion injury in cardiomyocytes.[62] miR-26a-5p modulates CTGF to attenuate acute LPS-induced ARDS.[63] These findings suggest that miR-26a-5p can modulate the inflammatory response in tissue injury, which is consistent with the functional characteristics of miR-26a-5p observed in this study. Our results indicated that miR-26a-5p extracted from SAT-EVs is involved in the regulation of intercellular communication and receptor cell function. Furthermore, this study provides the first evidence that miR-26a-5p in SAT-EVs regulates the dysregulated inflammatory response during ARDS progression. Therefore, targeting miR-26a-5p could potentially treat ARDS and warrants further investigation.

Bioinformatics predictions and dual-luciferase reporter assays showed that miR-26a-5p was transferred via SAT-EVs to directly regulate the expression of CHUK in receptor cells. CHUK, which encodes the subunit of the IκB kinase complex, IKKα, is a crucial regulator required for the activation of the NF-κB signaling pathway.[64] CHUK is involved in diverse biological processes, including proliferation, apoptosis, inflammation, and immune responses.[65–67] Downregulated levels of CHUK were found to ameliorate colitis in mice[68] and polarize microglia/macrophages towards an anti-inflammatory phenotype.[69] However, the relationship between CHUK and ARDS has not been sufficiently studied. In this study, the results showed that LPS stimulation increased CHUK expression, which enhanced pulmonary permeability and release of inflammatory cytokines and chemokines. Moreover, si-CHUK experiments and sequencing revealed that pro-inflammatory factors associated with the NF-κB pathway, such as IκBα, P65, IL-1β, and PTGS2, were enriched and downregulated in the si-CHUK group. In vivo and in vitro studies have shown that LPS treatment increased IκBα phosphorylation, the p-P65/P65 protein ratio, and protein levels of IL-1β, iNOS, and PTGS2. Meanwhile, we downregulated the expression of CHUK by upregulating its negative regulatory gene miR-26a-5p, resulting in a substantial decrease in the levels of pro-inflammatory factors associated with CHUK. These findings suggest that CHUK contributes to uncontrolled inflammation in ARDS. At the molecular level, CHUK activates phosphorylation and degradation of IκBα, triggering the release of NF-κB into the nucleus to activate pro-inflammatory gene transcription. Therefore, CHUK may be a novel molecular target for the management of ARDS, distinct from previously reported targets, such as HMGB1[70] or TLR4.[71]

Given the high degree of purification and self-cleaning properties of the lung tissue, the application of EVs in the treatment of ARDS is promising. The natural biocompatibility, high carrier capacity, and ease of engineering modification of EVs make them suitable for personalized treatments. Compared to other tissue sources, SAT-EVs can be more readily obtained in large quantities through liposuction, serving as an abundant and ethically sound source. Exosome therapy is expected to be widely used in the clinical setting. This study has some limitations. However, the signaling pathways mediating the protective effects of SAT-EVs in obesity have not yet been explored in detail. Pathways targeting the genes of SAT-EVs were enriched in metabolic and immune processes, which warrant further investigation.

Conclusion

In conclusion, our findings indicate that SAT-EVs can protect against ARDS. SAT-EVs delivered miR-26a-5p, targeting the CHUK/NF-κB pathway, which decreased excessive inflammatory responses in pulmonary macrophages and reduced the permeability of the alveolar capillary membrane (Figure 9). These findings offer a promising alternative for ARDS treatment and underscore the therapeutic potential of SAT-EVs in acellular therapy, particularly by modulating immune responses in ARDS.

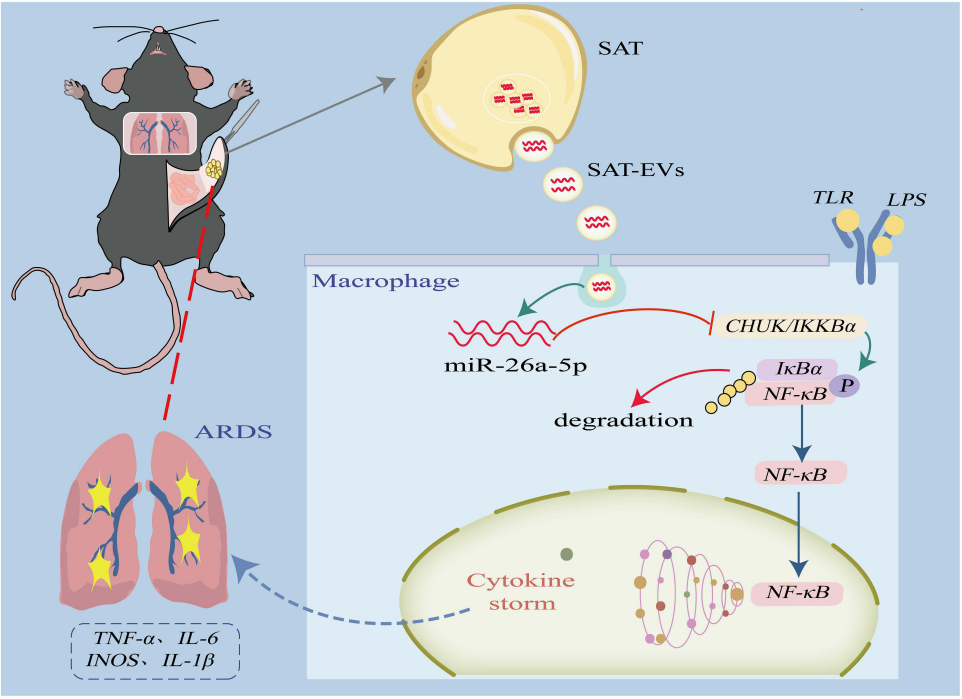

Figure 9 Schematic illustration of SAT-EVs–mediated regulation of ARDS via miR-26a-5p targeting the CHUK/NF-κB signaling pathway. SAT-EVs mitigate inflammation in ARDS by delivering miR-26a-5p to macrophages. miR-26a-5p targets CHUK, thereby inhibiting the phosphorylation of IκB-α and preventing NF-κB nuclear translocation. This pathway suppresses the expression of pro-inflammatory cytokines, including TNF-α, IL-1β, IL-6, and iNOS, ultimately alleviating the cytokine storm and attenuating ARDS-related lung injury.

Data Sharing Statement

Data supporting the findings of this study are available from the corresponding author (Gang Liu) upon reasonable request.

Ethical Statement

The animal study Protocol No approved by the Ethics Committee of University Town Hospital, Chongqing Medical University, Chongqing, China (protocol no. LL-DW-202407; Approval Date: June 11, 2024).

Acknowledgments

Xie Yu extends sincere gratitude to Fengming Chen for the steadfast spiritual support provided throughout the experimental process.

Author Contributions

All authors made a significant contribution to the work reported, whether that is in the conception, study design, execution, acquisition of data, analysis and interpretation, or in all these areas; took part in drafting, revising or critically reviewing the article; gave final approval of the version to be published; have agreed on the journal to which the article has been submitted; and agree to be accountable for all aspects of the work.\.

Funding

This study was supported by the Joint General Project of Science and Health in Chongqing (Grant Nos. 2022MSXM006, 2024ZYYB012, and 2023MSXM106), Chongqing Natural Science Foundation Innovation Development Joint Fund (Grant No. CSTB2023NSCQ-LZX0015), and Chongqing Natural Science Foundation (Grant No. 2024NSCQ-MSX0158).

Disclosure

The authors have no conflicts of interest to declare for this work.

References

1. Ning L, Shishi Z, Bo W, Huiqing L. Targeting immunometabolism against acute lung injury. *Clin Immunol*. 2023;249:109289. doi:10.1016/j.clim.2023.109289
2. Luyt CE, Bouadma L, Morris AC, et al. Pulmonary infections complicating ARDS. *Intensive Care Med*. 2020;46(12):2168–2183. doi:10.1007/s00134-020-06292-z
3. Scott TE, Kirkman E, Haque M, Gibb IE, Mahoney P, Hardman JG. Primary blast lung injury - a review. *Br J Anaesth*. 2017;118(3):311–316. doi:10.1093/bja/aew385
4. Sinha P, Meyer NJ, Calfee CS. Biological phenotyping in sepsis and acute respiratory distress syndrome. *Annu Rev Med*. 2023;74:457–471. doi:10.1146/annurev-med-043021-014005
5. He Q, Yin J, Zou B, Guo H. WIN55212-2 alleviates acute lung injury by inhibiting macrophage glycolysis through the miR-29b-3p/FOXO3/PFKFB3 axis. *Mol Immunol*. 2022;149:119–128. doi:10.1016/j.molimm.2022.06.005
6. Reeve T. Implementing guidelines about colorectal cancer: a national survey of target groups. *ANZ J Surg*. 2001;71(3):137–138. doi:10.1046/j.1440-1622.2001.02099.x
7. Kang A, Ye G, Afkhami S, et al. LPS-induced lung tissue-resident trained innate immunity provides differential protection against pneumococci and SARS-CoV-2. *Cell Rep*. 2024;43(10):114849. doi:10.1016/j.celrep.2024.114849
8. Peng X, Luo Z, He S, Zhang L, Li Y. Blood-brain barrier disruption by lipopolysaccharide and sepsis-associated encephalopathy. *Front Cell Infect Microbiol*. 2021;11:768108. doi:10.3389/fcimb.2021.768108
9. Almli CR, Fisher RS. Postnatal development of sensory influences on neurons in the ventromedial hypothalamic nucleus of the rat. *Brain Res*. 1985;350(1–2):13–26. doi:10.1016/0165-3806(85)90246-9
10. Zheng J, Mao H, Chong WP. Editorial: unraveling the molecular mechanisms of cytokine signaling in regulating inflammatory diseases. *Front Immunol*. 2025;16:1563469. doi:10.3389/fimmu.2025.1563469
11. Watabe Y, Giam chuang VT, Sakai H, et al. Carbon monoxide alleviates endotoxin-induced acute lung injury via NADPH oxidase inhibition in macrophages and neutrophils. *Biochem Pharmacol*. 2025;233:116782. doi:10.1016/j.bcp.2025.116782
12. Song Y, Lin W, Zhu W. Traditional Chinese medicine for treatment of sepsis and related multi-organ injury. *Front Pharmacol*. 2023;14:1003658. doi:10.3389/fphar.2023.1003658
13. Zheng J, Li Y, Kong X, Guo J. Exploring immune-related pathogenesis in lung injury: providing new insights into ALI/ARDS. *Biomed Pharmacother*. 2024;175:116773. doi:10.1016/j.biopha.2024.116773
14. Ahmadi Badi S, Tarashi S, Fateh A, Rohani P, Masotti A, Siadat SD. From the role of microbiota in gut-lung axis to SARS-CoV-2 pathogenesis. *Mediators Inflamm*. 2021;2021:6611222. doi:10.1155/2021/6611222
15. De Bandt JP, Obesity MC. Nutrients and the immune system in the era of COVID-19. *Nutrients*. 2021;13(2):610. doi:10.3390/nu13020610
16. Rosen ED, Spiegelman BM. What we talk about when we talk about fat. *Cell*. 2014;156(1–2):20–44. doi:10.1016/j.cell.2013.12.012
17. Di Maio G, Alessio N, Ambrosino A, Al Sammarraie SHA, Monda M, Di Bernardo G. Irisin influences the in vitro differentiation of human mesenchymal stromal cells, promoting a tendency toward beiging adipogenesis. *J Cell Biochem*. 2024;125(5):e30565. doi:10.1002/jcb.30565
18. Morigny P, Boucher J, Arner P, Langin D. Lipid and glucose metabolism in white adipocytes: pathways, dysfunction and therapeutics. *Nat Rev Endocrinol*. 2021;17(5):276–295. doi:10.1038/s41574-021-00471-8
19. Wang W, Seale P. Control of brown and beige fat development. *Nat Rev Mol Cell Biol*. 2016;17(11):691–702. doi:10.1038/nrm.2016.96
20. Hu Y, Huang Y, Jiang Y, Weng L, Cai Z, He B. The different shades of thermogenic adipose tissue. *Curr Obes Rep*. 2024;13(3):440–460. doi:10.1007/s13679-024-00559-y
21. Zwick RK, Guerrero-Juarez CF, Horsley V, Plikus MV. Anatomical, physiological, and functional diversity of adipose tissue. *Cell Metab*. 2018;27(1):68–83. doi:10.1016/j.cmet.2017.12.002
22. Reddy P, Lent-Schochet D, Ramakrishnan N, McLaughlin M, Jialal I. Metabolic syndrome is an inflammatory disorder: a conspiracy between adipose tissue and phagocytes. *Clin Chim Acta*. 2019;496:35–44. doi:10.1016/j.cca.2019.06.019
23. Choe SS, Huh JY, Hwang IJ, Kim JI, Kim JB. Adipose tissue remodeling: its role in energy metabolism and metabolic disorders. *Front Endocrinol*. 2016;7:30. doi:10.3389/fendo.2016.00030
24. Sakers A, De Siqueira MK, Seale P, Villanueva CJ. Adipose-tissue plasticity in health and disease. *Cell*. 2022;185(3):419–446. doi:10.1016/j.cell.2021.12.016
25. Johnston EK, Abbott RD. Adipose tissue paracrine-, autocrine-, and matrix-dependent signaling during the development and progression of obesity. *Cells*. 2023;12(3):407. doi:10.3390/cells12030407
26. Yang S, Sun Y, Yan C. Recent advances in the use of extracellular vesicles from adipose-derived stem cells for regenerative medical therapeutics. *J Nanobiotechnology*. 2024;22(1):316. doi:10.1186/s12951-024-02603-4
27. Wang J, Ji Y, Cao X, et al. Characterization and analysis of extracellular vesicle-derived miRNAs from different adipose tissues in mice. *Heliyon*. 2024;10(20):e39149. doi:10.1016/j.heliyon.2024.e39149
28. Cai L, Wang J, Yi X, et al. Nintedanib-loaded exosomes from adipose-derived stem cells inhibit pulmonary fibrosis induced by bleomycin. *Pediatr Res*. 2024;95(6):1543–1552. doi:10.1038/s41390-024-03024-7
29. Wang J, Chen ZJ, Zhang ZY, et al. Manufacturing, quality control, and GLP-grade preclinical study of nebulized allogenic adipose mesenchymal stromal cells-derived extracellular vesicles. *Stem Cell Res Ther*. 2024;15(1):95. doi:10.1186/s13287-024-03708-1
30. Wang J, Chen J, Sen S. MicroRNA as biomarkers and diagnostics. *J Cell Physiol*. 2016;231(1):25–30. doi:10.1002/jcp.25056
31. Castaño C, Kalko S, Novials A, Párrizas M. Obesity-associated exosomal miRNAs modulate glucose and lipid metabolism in mice. *Proc Natl Acad Sci U S A*. 2018;115(48):12158–12163. doi:10.1073/pnas.1808855115
32. Yang J, Huang X, Yu Q, et al. Extracellular vesicles derived from M2-like macrophages alleviate acute lung injury in a miR-709-mediated manner. *J Extracell Vesicles*. 2024;13(4):e12437. doi:10.1002/jev2.12437

33. Cai B, Song W, Chen S, et al. Bone mesenchymal stem cell-derived small extracellular vesicles ameliorated lipopolysaccharide-induced lung injury via the miR-21-5p/PCSK6 pathway. *J Immunol Res*. 2023;2023:3291137. doi:10.1155/2023/3291137
34. Sun J, Liao Z, Li Z, et al. Down-regulation miR-146a-5p in Schwann cell-derived exosomes induced macrophage M1 polarization by impairing the inhibition on TRAF6/NF-κB pathway after peripheral nerve injury. *Exp Neurol*. 2023;362:114295. doi:10.1016/j.expneurol.2022.114295
35. Théry C, Witwer KW, Aikawa E, et al. Minimal information for studies of extracellular vesicles 2018 (MISEV2018): a position statement of the international society for extracellular vesicles and update of the MISEV2014 guidelines. *J Extracell Vesicles*. 2018;7(1):1535750. doi:10.1080/20013078.2018.1535750
36. Zhang H, Lu H, Yu L, et al. Effects of gestational exposure to perfluorooctane sulfonate on the lung development of offspring rats. *Environ Pollut*. 2021;272:115535. doi:10.1016/j.envpol.2020.115535
37. Zhu Y, Han Q, Wang L, et al. Jinhua qinggan granules attenuates acute lung injury by promotion of neutrophil apoptosis and inhibition of TLR4/MyD88/NF-κB pathway. *J Ethnopharmacol*. 2023;301:115763. doi:10.1016/j.jep.2022.115763
38. Chakraborty S, Singh A, Wang L, et al. Trained immunity of alveolar macrophages enhances injury resolution via KLF4-MERTK-mediated efferocytosis. *J Exp Med*. 2023;220(11). doi:10.1084/jem.20221388
39. Chen HH, Li HF, Tseng TL, Lin H. Perivascular adipose tissue and adipocyte-derived exosomal miRNAs maintain vascular homeostasis. *Heliyon*. 2023;9(12):e22607. doi:10.1016/j.heliyon.2023.e22607
40. Wang M, Min M, Duan H, Mai J, Liu X. The role of macrophage and adipocyte mitochondrial dysfunction in the pathogenesis of obesity. *Front Immunol*. 2024;15:1481312. doi:10.3389/fimmu.2024.1481312
41. Trim WV, Lynch L. Immune and non-immune functions of adipose tissue leukocytes. *Nat Rev Immunol*. 2022;22(6):371–386. doi:10.1038/s41577-021-00635-7
42. Jacks RD, Lumeng CN. Macrophage and T cell networks in adipose tissue. *Nat Rev Endocrinol*. 2024;20(1):50–61. doi:10.1038/s41574-023-00908-2
43. Zhou Z, Tao Y, Zhao H, Wang Q. Adipose extracellular vesicles: messengers from and to macrophages in regulating immunometabolic homeostasis or disorders. *Front Immunol*. 2021;12:666344. doi:10.3389/fimmu.2021.666344
44. Hornung F, Schulz L, Köse-Vogel N, et al. Thoracic adipose tissue contributes to severe virus infection of the lung. *Int J Obes*. 2023;47(11):1088–1099. doi:10.1038/s41366-023-01362-w
45. Xu DL, Zhao MX. Leptin mediates the suppressive effect of partial fat removal on cellular and humoral immunity in striped hamsters. *Comp Biochem Physiol a Mol Integr Physiol*. 2022;271:111256. doi:10.1016/j.cbpa.2022.111256
46. Song JW, Lam SM, Fan X, et al. Omics-driven systems interrogation of metabolic dysregulation in COVID-19 Pathogenesis. *Cell Metab*. 2020;32(2):188–202.e5. doi:10.1016/j.cmet.2020.06.016
47. Thomou T, Mori MA, Dreyfuss JM, et al. Adipose-derived circulating miRNAs regulate gene expression in other tissues. *Nature*. 2017;542(7642):450–455. doi:10.1038/nature21365
48. Fatima F, Nawaz M. Long distance metabolic regulation through adipose-derived circulating exosomal miRNAs: a trail for RNA-based therapies? *Front Physiol*. 2017;8:545. doi:10.3389/fphys.2017.00545
49. Chen SY, Chen YL, Li PC, et al. Engineered extracellular vesicles carrying let-7a-5p for alleviating inflammation in acute lung injury. *J Biomed Sci*. 2024;31(1):30. doi:10.1186/s12929-024-01019-4
50. Sun L, Sun M, Ma K, Liu J. Let-7d-5p suppresses inflammatory response in neonatal rats with necrotizing enterocolitis via LGALS3-mediated TLR4/NF-κB signaling pathway. *Am J Physiol Cell Physiol*. 2020;319(6):C967–c979. doi:10.1152/ajpcell.00571.2019
51. Zhang H, Gu XN, Wei MJ, Ji LL. Discovery of miRNA and target signal molecules involved in inhibition of chlorogenic acid on N-acetyl-p-aminophenol-induced hepatotoxicity based on microRNA array. *Zhongguo Zhong Yao Za Zhi*. 2023;48(4):1014–1022. doi:10.19540/j.cnki.cjcmm.20221017.401
52. Zhang Q, Liu Y, Yuan Y, et al. miR-26a-5p protects against drug-induced liver injury via targeting Bid. *Toxicol Mech Methods*. 2022;32(5):325–332. doi:10.1080/15376516.2021.2003919
53. Xing X, Guo S, Zhang G, et al. miR-26a-5p protects against myocardial ischemia/reperfusion injury by regulating the PTEN/PI3K/AKT signaling pathway. *Braz J Med Biol Res*. 2020;53(2):e9106. doi:10.1590/1414-431x20199106
54. Zhu WJ, Yan Y, Zhang JW, Tang YD, Han B. Effect and mechanism of miR-26a-5p on proliferation and apoptosis of hepatocellular carcinoma cells. *Cancer Manag Res*. 2020;12:3013–3022. doi:10.2147/cmar.S237752
55. Li M, Xiao Y, Liu M, et al. MiR-26a-5p regulates proliferation, apoptosis, migration and invasion via inhibiting hydroxysteroid dehydrogenase like-2 in cervical cancer cell. *BMC Cancer*. 2022;22(1):876. doi:10.1186/s12885-022-09970-x
56. Ding N, Wang W, Teng J, et al. miR-26a-5p regulates adipocyte differentiation via directly targeting ACSL3 in adipocytes. *Adipocyte*. 2023;12(1):1–10. doi:10.1080/21623945.2023.2166345
57. Coban N, Erkan AF, Ozuynuk-Ertugrul AS, Ekici B. Investigation of miR-26a-5p and miR-19a-3p expression levels in angiographically confirmed coronary artery disease. *Acta Cardiol*. 2023;78(8):945–956. doi:10.1080/00015385.2023.2227484
58. Shi R, Chen L, Wang W, et al. Plasma miR-26a-5p is a biomarker for retinal neurodegeneration of early diabetic retinopathy. *Eye*. 2021;35(6):1587–1599. doi:10.1038/s41433-021-01393-5
59. Chen Y, Zhou X, Wu Y. The miR-26a-5p/IL-6 axis alleviates sepsis-induced acute kidney injury by inhibiting renal inflammation. *Ren Fail*. 2022;44(1):551–561. doi:10.1080/0886022x.2022.2056486
60. Ren M, Wang T, Han Z, Fu P, Liu Z, Ouyang C. Long noncoding RNA OIP5-AS1 contributes to the progression of atherosclerosis by targeting miR-26a-5p through the AKT/NF-κB pathway. *J Cardiovasc Pharmacol*. 2020;76(5):635–644. doi:10.1097/fjc.0000000000000889
61. Wang D, Zhou Z, Yuan L. Polydatin reverses oxidation low lipoprotein (oxLDL)-induced apoptosis of human umbilical vein endothelial cells via regulating the miR-26a-5p/Bid axis. *Eur J Histochem*. 2022;66(4). doi:10.4081/ejh.2022.3505
62. Yan G, Wang J, Fang Z, Yan S, Zhang Y. MiR-26a-5p targets WNT5A to protect cardiomyocytes from injury due to hypoxia/reoxygenation through the Wnt/β-catenin signaling pathway. *Int Heart J*. 2021;62(5):1145–1152. doi:10.1536/ihj.21-054
63. Li H, Yang T, Fei Z. miR-26a-5p alleviates lipopolysaccharide-induced acute lung injury by targeting the connective tissue growth factor. *Mol Med Rep*. 2021;23(1). doi:10.3892/mmr.2020.11643
64. Paul A, Edwards J, Pepper C, Mackay S. Inhibitory-κB Kinase (IKK) α and nuclear factor-κB (NFκB)-inducing kinase (NIK) as anti-cancer drug targets. *Cells*. 2018;7(10):176. doi:10.3390/cells7100176

65. Liao J, Qin QH, Lv FY, et al. IKKα inhibition re-sensitizes acquired Adriamycin-resistant triple negative breast cancer cells to chemotherapy-induced apoptosis. *Sci Rep*. 2023;13(1):6211. doi:10.1038/s41598-023-33358-x
66. Li F, Liang H, You H, et al. Targeting HECTD3-IKKα axis inhibits inflammation-related metastasis. *Signal Transduct Target Ther*. 2022;7(1):264. doi:10.1038/s41392-022-01057-0
67. Huang B, Zhang L, Xu F, et al. Oyster versatile IKKα/βs are involved in toll-like receptor and RIG-I-like receptor signaling for innate immune response. *Front Immunol*. 2019;10:1826. doi:10.3389/fimmu.2019.01826
68. Xue L, Jin X, Ji T, et al. Luteolin ameliorates DSS-induced colitis in mice via suppressing macrophage activation and chemotaxis. *Int Immunopharmacol*. 2023;124(Pt B):110996. doi:10.1016/j.intimp.2023.110996
69. Li X, Xia Q, Mao M, et al. Annexin-A1 SUMOylation regulates microglial polarization after cerebral ischemia by modulating IKKα stability via selective autophagy. *Sci Adv*. 2021;7(4). doi:10.1126/sciadv.abc5539
70. He F, Gu L, Cai N, et al. The HMGB1-RAGE axis induces apoptosis in acute respiratory distress syndrome through PERK/eIF2α/ATF4-mediated endoplasmic reticulum stress. *Inflamm Res*. 2022;71(10–11):1245–1260. doi:10.1007/s00011-022-01613-y
71. Shirey KA, Blanco JCG, Vogel SN. Targeting TLR4 signaling to blunt viral-mediated acute lung injury. *Front Immunol*. 2021;12:705080. doi:10.3389/fimmu.2021.705080